ACS APPLIED MATERIALS & INTERFACES

Research Article

www.acsami.org

Facile One-Pot Solvothermal Method to Synthesize Sheet-on-Sheet Reduced Graphene Oxide (RGO)/$ZnIn_2S_4$ Nanocomposites with Superior Photocatalytic Performance

Lin Ye, Jinlong Fu, Zhen Xu, Rusheng Yuan, and Zhaohui Li*

Research Institute of Photocatalysis, State Key Laboratory of Photocatalysis on Energy and Environment, College of Chemistry and Chemical Engineering, Fuzhou University, Fuzhou 350002, P. R. China

Supporting Information

ABSTRACT: Highly reductive RGO (reduced graphene oxide)/$ZnIn_2S_4$ nanocomposites with a sheet-on-sheet morphology have been prepared via a facile one-pot solvothermal method in a mixture of *N*,*N*-dimethylformamide (DMF) and ethylene glycol (EG) as solvent. A reduction of GO (graphene oxide) to RGO and the formation of $ZnIn_2S_4$ nanosheets on highly reductive RGO has been simultaneously achieved. The effect of the solvents on the morphology of final products has been investigated and the formation mechanism was proposed. The as-prepared RGO/$ZnIn_2S_4$ nanoscomposites were characterized by powder X-ray diffraction (XRD), Fourier transform infrared spectroscopy (FT-IR), Raman spectroscopy, X-ray photoelectron spectroscopy (XPS), N_2-adsorption BET surface area, UV−vis diffuse reflectance spectroscopy (DRS), scanning electron microscopy (SEM), transmission electron microscopy (TEM), high-resolution transmission electron microscopy (HRTEM). The photocatalytic activity for hydrogen evolution under visible light irradiations over the as-prepared RGO/$ZnIn_2S_4$ nanocomposites has been investigated. The as-prepared RGO/$ZnIn_2S_4$ nanocomposites show enhanced photocatalytic activity for hydrogen evolution under visible light irradiations and an optimum photocatalytic activity is observed over 1.0 wt % RGO incorporated $ZnIn_2S_4$ nanocomposite. The superior photocatalytic performance observed over RGO/$ZnIn_2S_4$ nanocomposites can be ascribed to the existence of highly reductive RGO which has strong interactions with $ZnIn_2S_4$ nanosheets. The existence of the strong interaction between $ZnIn_2S_4$ nanosheets and RGO in the nancomposites facilitates the electron transfer from $ZnIn_2S_4$ to RGO, with the latter serving as a good electron acceptor, mediator as well as the co-catalyst for hydrogen evolution. This study can provide some guidance for us in the developing of RGO-incorporated nanocomposite photocatalysts.

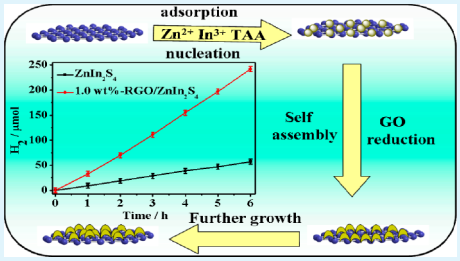

KEYWORDS: *$ZnIn_2S_4$, RGO, photocatalytic, hydrogen evolution, visible light*

1. INTRODUCTION

The ever-increasing global demand for energy has stimulated a new wave of research activities on efficient utilization of solar energy. Semiconductor-based photocatalytic hydrogen generation is considered to be an attractive and promising strategy in solving the increasing serious energy and environmental problems since it can utilize the solar energy and is environmental friendly.[1,2] Ever since the pioneering work of a photoelectrochemical cell using Pt−TiO_2 electrodes for water splitting by Fujishima and Honda in 1972, great efforts have been devoted to the development of highly efficient semiconductor photocatalysts for hydrogen production.[3] So far, a variety of active photocatalysts for hydrogen production, including metal oxides, sulfides, oxynitrides, as well as the metal-free semiconductors have already been developed.[4−10]

Among the numerous types of semiconductor systems studied, metal sulfides have demonstrated promising activities towards hydrogen evolution from water containing sacrificial reagents under visible light.[5,11−13] $ZnIn_2S_4$ is a ternary chalcogenide with a suitable band gap (2.34−2.48 eV), well corresponding to the visible light absorption.[7,8,14] $ZnIn_2S_4$ exhibits two distinct polymorphs based on cubic and hexagonal lattices, which can be controlled synthesized via a facile hydrothermal method using different precursors.[15,16] Previous studies revealed that both polymorphs of $ZnIn_2S_4$ are active for photocatalytic hydrogen generation under visible light irradiations and show considerable chemical stability.[7,8,17,18] However, the photocatalytic hydrogen evolution activity over pure $ZnIn_2S_4$ is low because of the poor separation efficiency and low migration ability of the photoexcited charge carriers. To enhance the photocatalytic performance of $ZnIn_2S_4$, a variety of efforts have been made, for example, doping with metals, such as Cu, incorporation of multiwalled carbon nanotubes (MWCNTs), RGO (reduced graphene oxide), or polymers.[8,19−21]

Graphene, an allotrope of carbon, is a two-dimensional (2D) sp^2 carbon network. Because of its many fascinating properties such as large surface area, high electrical conductivity, stability

Received: December 6, 2013
Accepted: February 18, 2014
Published: February 18, 2014

   dx.doi.org/10.1021/am5004415 | ACS Appl. Mater. Interfaces 2014, 6, 3483−3490

and tunable surface properties, graphene has attracted a wide range of recent interests.[22−24] Most of the previous studies have found that the performance of the semiconductor photocatalysts can be enhanced by the incorporation of RGO.[25−28] However, our recent study revealed that there exists a correlation between the reductive degree of RGO and the photocatalytic activity in the RGO/semiconductor nanocomposites.[8] For example, our previous study found that the hydrothermally prepared RGO/$ZnIn_2S_4$ nanocomposite, which incorporates RGO with a lower reductive degree, exhibits lower photocatalytic activity for hydrogen evolution even when compared to pure $ZnIn_2S_4$. However, when the hydrothermally prepared RGO/$ZnIn_2S_4$ nanocomposite was further treated with photoreduction or hydrazine to increase the reduction degree of RGO, the as-formed products show significantly enhanced performance for hydrogen evolutions. This study indicates that it is important to develop RGO/semiconductor nanocomposites with RGO in a highly reductive degree for their better application in photocatalysis.

In this manuscript, a facile one-pot solvothermal method has been developed to prepare RGO/$ZnIn_2S_4$ nanocomposites with a sheet-on-sheet morphology. A simultaneous reduction of GO (graphene oxide) to highly reductive RGO and the formation of $ZnIn_2S_4$ nanosheets on the as-formed RGO have been achieved via a solvothermal reaction using a mixture of ethylene glycol (EG) and *N*,*N*-dimethylformamide (DMF) as solvent. The as-prepared RGO/$ZnIn_2S_4$ nanocomposites exhibited highly enhanced photocatlaytic activity for hydrogen evolution under visible light irradiations and an optimum photocatalytic activity was observed over 1.0 wt % RGO incorporated $ZnIn_2S_4$ nanocomposite. The superior photocatalytic performance observed over RGO/$ZnIn_2S_4$ nanocomposites can be ascribed to the existence of the highly reductive RGO with strongly interactions to $ZnIn_2S_4$ nanosheets. The existence of the strong interaction between $ZnIn_2S_4$ nanosheets and RGO in the nancomposites facilitates the electron transfer from $ZnIn_2S_4$ to RGO, with the latter serving as a good electron acceptor, mediator as well as the co-catalyst for hydrogen evolution.

2. EXPERIMENTAL SECTION

2.1. Preparations. All the reagents are analytical grade and used without further purifications. GO was synthesized following the Hummers' method with a slight modification.[28] For the synthesis of RGO/$ZnIn_2S_4$ nanocomposites, different amounts of GO were dispersed in a mixed solution containing 30 mL of DMF and 30 mL of EG, followed by ultrasonication for 60 min. Then $ZnCl_2$ (0.136 g, 1 mmol) and $InCl_3.4H_2O$ (0.586 g, 2 mmol) was added to the GO dispersion and the suspension continued to ultrasonicate for a few minutes. After that, thioacetamide (TAA, 0.3 g, 4 mmol) was added into the mixture under vigorous stirring. The resultant suspension was transferred to a 100 mL Teflon liner, sealed in the stainless steel autoclave and heated at 200 °C for 24 h. After the autoclave was cooled to room temperature, the products were collected and washed with de-ionized water and ethanol for several times and dried at 60 °C. The RGO/$ZnIn_2S_4$ nanocomposites with different amount of RGO are denoted as *x* wt%-RGO/$ZnIn_2S_4$. For comparison, pure $ZnIn_2S_4$ was also synthesized by a similar solvothermal reaction in absence of GO (Supporting Information Figure S1).

2.2. Characterizations. Powder X-ray diffraction (XRD) data were collected using a Bruker D8 Advance X-ray diffractometer (Cu K_α irradiations). Raman spectroscopy was performed using an invia-Reflex Micro-Raman Spectroscopy system (Renishaw Co.) with 532 nm line of an Ar ion laser at room temperature. The IR analyses were carried out on a Nicolet 670 FT-IR spectrometer. The morphology of the samples was characterized by a field emission scanning electron microscopy (SEM) (JSM-6700F). The transmission electron microscopy (TEM) and high resolution transmission electron microscopy (HRTEM) images were obtained in a JEOL model JEM 2010 EX instrument at an accelerating voltage of 200 kV. The powder particles were supported on a carbon film coated on a 3 mm diameter fine-mesh copper grid. The sample suspension in ethanol was sonicated and a drop was dripped on the support film. X-ray photoelectron spectroscopy (XPS) measurements were performed on a PHI Quantum 2000 XPS system (PHI, USA) with a monochromatic Al Kα source and a charge neutralizer. All the binding energy is reference to C 1s peak observed in the XPS spectrum of pure $ZnIn_2S_4$. BET surface area was carried out on an ASAP2020M apparatus (Micromeritics Instrument Corp., USA). For BET surface area analyses, the samples were degassed in vacuum at 200 °C for 10 h and then measured at 77 K. UV−visible diffuse reflectance spectra (UV-DRS) of the powders were obtained for the dry-pressed disk samples using a Cary 500 Scan Spectrophotometer (Varian, USA). $BaSO_4$ was used as a reflectance standard in the UV−visible diffuse reflectance experiment. Electrochemical impedance spectroscopy (EIS) were measured on an electrochemical analyzer (Zahner, Germany) in a standard three-electrode system using the prepared samples as the working electrodes with an active area of ~0.25 cm^2, a Pt wire as the counter electrode, and Ag/AgCl (saturated KCl) as a reference electrode. Na_2SO_4 (0.2 M) aqueous solution was used as the electrolyte. Impedance data were fitted with ZSimpWin software (Princeton Applied Research). Photoluminescence (PL) spectra were carried out on a fluorescence spectrometer (Hitachi F-4500). The PL emission spectra of pure $ZnIn_2S_4$ and RGO/$ZnIn_2S_4$ with different amount of RGO were obtained respectively with a 260 nm wavelength as the excitation source.

2.3. Photocatalytic Hydrogen Evolution. Photocatalytic experiments for hydrogen evolution were carried out in a closed gas circulation and evacuation system fitted with a top Pyrex window. 50 mg of photocatalyst was dispersed in 100 mL of aqueous solution containing 2.0 mL of lactic acid as sacrificial reagents. The suspension was irradiated with a 300 W Xe lamp equipped with a 420 nm cut-off filter to provide the visible light irradiations. The temperature of the reactant solution was maintained at room temperature by a flow of cooling water during the photocatalytic reaction. The amount of hydrogen evolved was determined with an on-line gas chromatograph equipped with a TCD detector.

3. RESULTS AND DISCUSSION

RGO/$ZnIn_2S_4$ nanocomposites were prepared via one-pot solvothermal method from $ZnCl_2$, $InCl_3$ and TAA in the presence of different amounts of GO using a mixed solvent of DMF and EG in 1:1 ratio. As shown in the XRD patterns of the as-prepared RGO/$ZnIn_2S_4$ nanocomposites, all the as-prepared samples show characteristic peaks assigned to (006), (102), (104), (108), and (110) crystallographic planes of hexagonal $ZnIn_2S_4$ phase (JCPDS-03-065-2023), indicating that the presence of RGO does not influence the structure of $ZnIn_2S_4$ (Figure 1). No diffractions peaks corresponding to either GO or RGO has been observed in the XRD patterns of the resultant products because of its low amount and relatively low diffraction intensity.[29] However, the existence of RGO in the nanocomposite can be confirmed by the FT-IR spectra. As shown in Figure 2, only two peaks at 1610 and 1396 cm^{-1} corresponding to the surface absorbed water molecules and hydroxyl groups are observed over $ZnIn_2S_4$.[30] On the contrary, RGO/$ZnIn_2S_4$ nanocomposites show peaks at 1048, 1620 and 1450 cm^{-1} corresponding to the C−O stretching vibrations, skeletal vibration of graphene and O−H deformation respectively. The peak at 1735 cm^{-1} which assigned to C═O vibration observed on GO totally disappears in the RGO/$ZnIn_2S_4$ nanocomposites, indicating that GO has been successfully reduced to RGO during the solvothermal

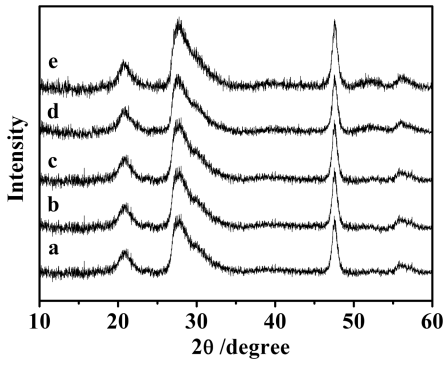

Figure 1. XRD patterns of (a) $ZnIn_2S_4$, (b) 0.5 wt %-RGO/$ZnIn_2S_4$, (c) 1.0 wt %-RGO/$ZnIn_2S_4$, (d) 3.0 wt %-RGO/$ZnIn_2S_4$, and (e) 5.0 wt %-RGO/$ZnIn_2S_4$ nanocomposites.

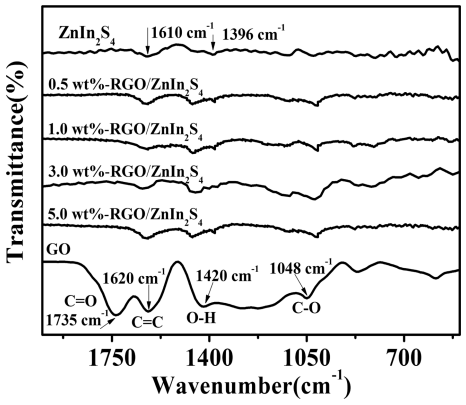

Figure 2. FTIR spectra of GO, $ZnIn_2S_4$, and RGO/$ZnIn_2S_4$ nanocomposites with different amount of RGO.

reaction.[31] The presence of the RGO in the nanocomposites is also confirmed by the Raman spectroscopy (Figure 3). All the

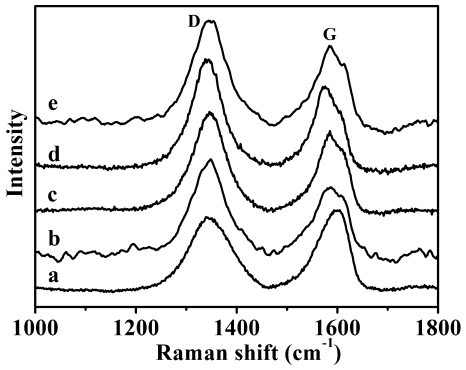

Figure 3. Raman spectra of (a) GO, (b) 0.5 wt %-RGO/$ZnIn_2S_4$, (c) 1.0 wt %-RGO/$ZnIn_2S_4$, (d) 3.0 wt %-RGO/$ZnIn_2S_4$, and (e) 5.0 wt %-RGO/$ZnIn_2S_4$ nanocomposites.

samples show characteristic peaks at 1346 and 1596 cm^{-1}, corresponding to the D and G bands of RGO respectively. The ratio of I_D/I_G over the nanocomposites is determined to be ~1.29, much higher than that observed over the original GO (0.91). Since the ratio of I_D/I_G is an indicator of the graphitization degree of carbonaceous materials, the higher I_D/I_G observed over the as-prepared nanocomposites as compared to that of GO suggests a successful reduction of GO to RGO in the nanocomposites.[32]

XPS analyses were carried out to study the surface chemical composition and electronic state of 1.0 wt %-RGO/$ZnIn_2S_4$ nanocomposite. Characteristic binding energy of 1021.4 and 1044.7 eV for Zn^{2+} 2p, 445.3 and 452.9 eV for In^{3+} 3d, and 161.6 eV for S^{2-} 2p are observed over RGO/$ZnIn_2S_4$ nanocomposite. As compared to those observed over pure $ZnIn_2S_4$, the peaks of Zn 2p and S 2p in RGO/$ZnIn_2S_4$ nanocomposite shift toward lower binding energy, while a higher binding energy shift is observed for In 3d. The shift of the binding energy for RGO/$ZnIn_2S_4$ nanocomposite as compared to pure $ZnIn_2S_4$ suggests a strong electronic interaction between RGO and $ZnIn_2S_4$ in the nanocomposite (Figure 4a–c).[33] The XPS spectrum of the RGO/$ZnIn_2S_4$ nanocomposite in the C 1s region shows three peaks at 284.8, 285.6, and 286.6 eV. The peaks at 284.8 and 286.6 eV can be assigned to the sp^2-hybridized carbon (C–C) and epoxy/hydroxyl carbon (C–O) respectively.[34,35] As compared to original GO, the intensity of the peak ascribed to the epoxy/hydroxyls carbon (C–O) (286.8 eV) in the nanocomposite significantly decreases, while the peak corresponding to the carboxyl (C═O) (288.5 eV) totally disappears, in consistent with the FT-IR result. A small additional peak at 285.6 eV can be assigned to the C–N bond, which may be induced by the residue DMF from the solvent. The O-bound C content for 1.0 wt %-RGO/$ZnIn_2S_4$ nanocomposite decreases from the original 55.0% in GO to 14.0%, indicating that the one-pot solvothermal treatment can lead to RGO/$ZnIn_2S_4$ nanocomposites with RGO in a highly reductive degree.[36]

The morphology of the as-prepared RGO/$ZnIn_2S_4$ nanocomposites was studied by SEM and TEM. Two-dimensional flakelike structure is observed in the SEM image of a typical 1.0 wt %-RGO/$ZnIn_2S_4$ nanocomposite (Figure 5a). The flakelike morphology is quite different from the RGO/$ZnIn_2S_4$ microspheres prepared via a hydrothermal method which we reported previously, indicating that the reaction solvent plays an important role for the morphology formation.[8] The TEM image of the 1.0 wt %-RGO/$ZnIn_2S_4$ nanocomposite clearly shows that ultrathin $ZnIn_2S_4$ nanosheets are dispersed on RGO sheet. These $ZnIn_2S_4$ nanosheets are interconnected with each other to form a sheet-on-sheet RGO/$ZnIn_2S_4$ nanocomposite (Fig. 5b). Well-defined crystal structure of hexagonal $ZnIn_2S_4$ in the RGO/$ZnIn_2S_4$ nanocomposites is evidenced from the HRTEM image. Clear lattice-fringe spacing of 0.32 nm can be assigned to the (102) crystal plane of hexagonal phase of $ZnIn_2S_4$ (Figure 5c). The energy dispersed spectrum (EDS) also reveals the co-existence of Zn, In, and S, confirmation of the formation of $ZnIn_2S_4$ (Figure 5d).

The mechanism for the formation of the RGO/$ZnIn_2S_4$ nanocomposites with a sheet-on-sheet is illustrated in Scheme 1. It is well known that GO has lots of hydrophilic functional groups (e.g.,–OH, –COOH) on its surface,[37] which can act as the adsorption sites for Zn^{2+} and In^{3+} ions. These surface adsorbed Zn^{2+} and In^{3+} cations can react with EG to form metal glycolate complex, which further interact with S^{2-} anions provided by the decomposition of the thioacetamide (TAA) to form $ZnIn_2S_4$ nuclei on the GO surface.[17,38] As a result of the intrinsic lamellar structure of the hexagonal $ZnIn_2S_4$ phase, the as-formed $ZnIn_2S_4$ nuclei tend to grow larger and form the nanosheets on the surface as the reaction continued. In the meantime, GO is reduced to RGO by the organic solvent.[39] Finally, these $ZnIn_2S_4$ nanosheets grew larger and interconnect with each other to form the sheet-on-sheet hierarchical RGO/$ZnIn_2S_4$ nanocomposites. Controlled experiments performed in

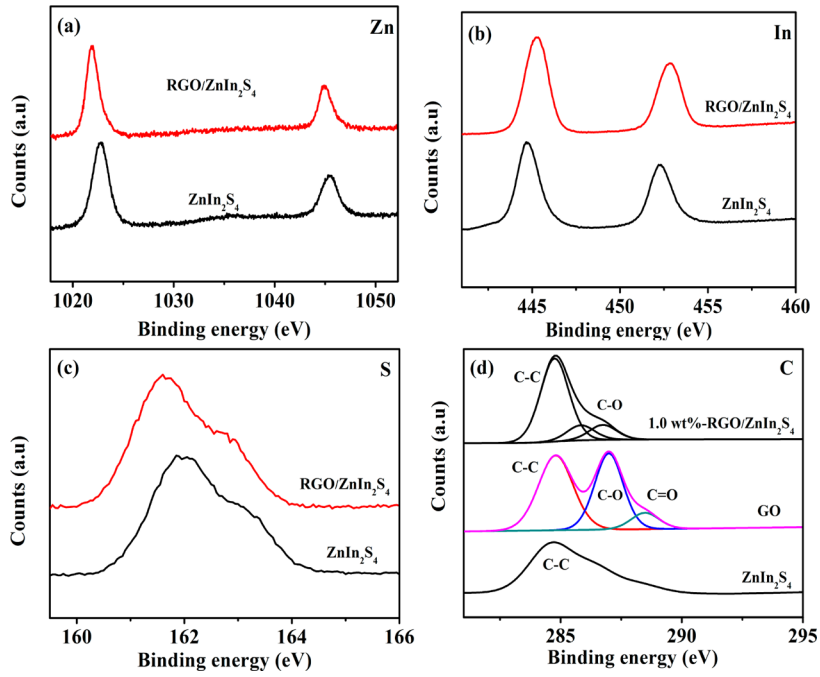

Figure 4. XPS spectra of (a) Zn 2p, (b) In 3d, and (c) S 2p in $ZnIn_2S_4$ and 1.0 wt %-RGO/$ZnIn_2S_4$ nanocomposite. (d) XPS spectra in C1s region for 1.0 wt %-RGO/$ZnIn_2S_4$ nanocomposite, GO, and $ZnIn_2S_4$ nanocomposite.

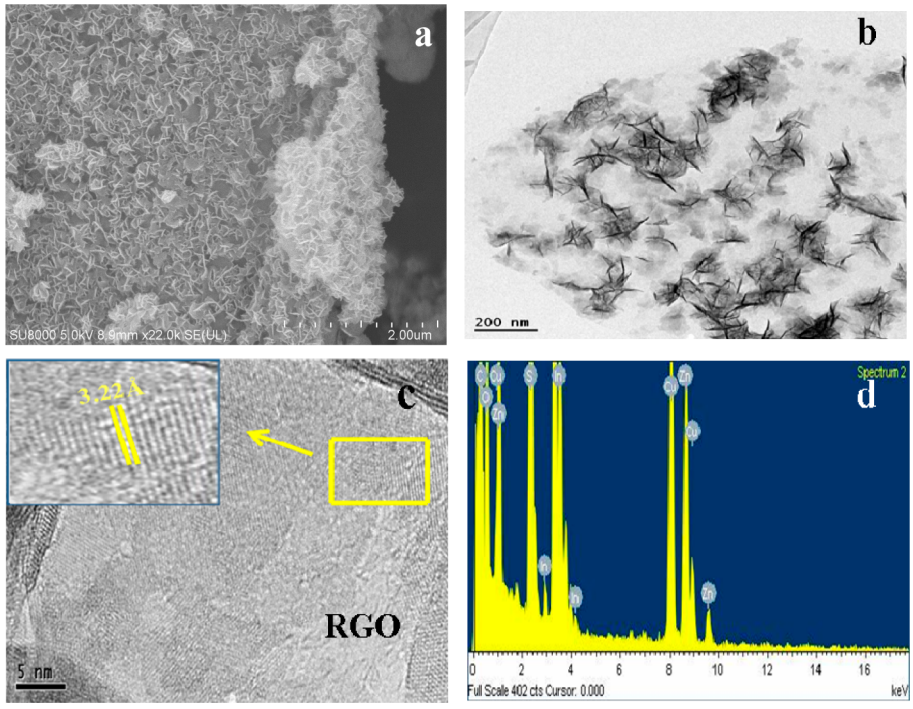

Figure 5. 1.0 wt %-RGO/$ZnIn_2S_4$ nanocomposite (a) SEM image, (b) low magnification TEM image, (c) HRTEM image, and (d) EDS.

absence of EG (i.e., in pure DMF) only gave product composed of phase separated RGO and $ZnIn_2S_4$ as shown in Supporting Information Figure S2. This indicates that the formation of the metal glycolate complex between EG and the metal ions is important for the formation of RGO/$ZnIn_2S_4$ nanocomposites with strong interaction. On the contrary, pure EG in absence of DMF also cannot lead to high qualified RGO/$ZnIn_2S_4$ nanocomposites with uniform flakelike morphology as shown in Supporting Information Figure S3. Previous work has shown that homogeneous colloidal suspension of RGO could be produced in DMF.[40,41] Therefore the use of DMF is supposed to impede the aggregation of RGO, which would favor the dispersion of Zn^{2+} and In^{3+} absorbed on the surface of RGO sheet. The above controlled experiments clearly indicate that both EG and DMF are indispensable for the formation of the sheet-on-sheet hierarchical RGO/$ZnIn_2S_4$ nanocomposites. The formation mechanism was confirmed by the result from the time-dependent experiments. As shown in Supporting Information Figure S4, after reacting for 1 h, small nanoparticles of $ZnIn_2S_4$ formed on the RGO surface. When the

dx.doi.org/10.1021/am5004415 | ACS Appl. Mater. Interfaces 2014, 6, 3483−3490

Scheme 1. Proposed Mechanism for the Formation of RGO/$ZnIn_2S_4$ Nanocomposite with a Sheet-on-Sheet Morphology

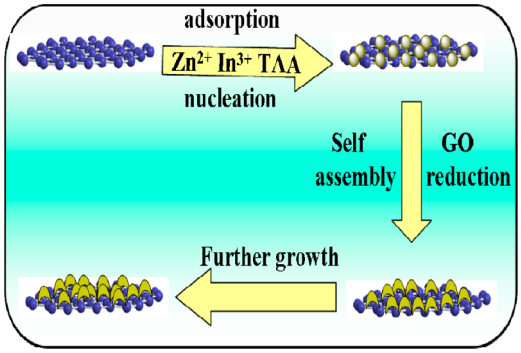

reaction time was prolonged to 10 h, small nanoparticles disappeared and small nanosheets of $ZnIn_2S_4$ formed. When the reaction time was prolonged to 24 h, these small nnaosheets grew larger and interconnected with each other.

The nitrogen adsorption/desorption isotherms of 1.0 wt %-RGO/$ZnIn_2S_4$ nanocomposite exhibits stepwise adsorption and desorption behavior as shown in Figure 6. The BET

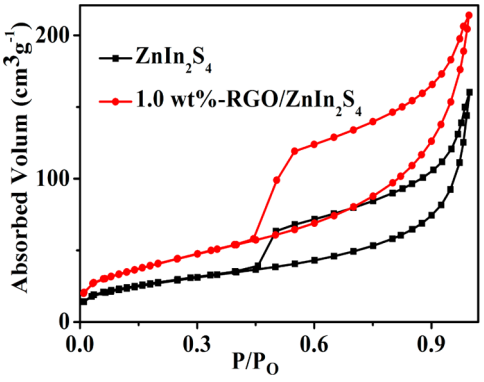

Figure 6. Nitrogen adsorption−desorption isotherms of 1.0 wt %-RGO/$ZnIn_2S_4$ nanocomposite and $ZnIn_2S_4$.

specific surface area is determined to be 150.0 cm^3 g^{-1}, higher than that observed over pure $ZnIn_2S_4$ (99.8 cm^3 g^{-1}). The higher BET specific surface area of RGO/$ZnIn_2S_4$ nanocomposite as compared to pure $ZnIn_2S_4$ can be attributed to the introduction of RGO with an extremely high surface area, as well as the uniform grown of ultrathin $ZnIn_2S_4$ nanosheets on the surface of RGO. The large surface area of heterogeneous photocatalysis can provide more surface active sites for the adsorption of reactant molecules, making the photocatalytic process more efficient.

The UV−visible diffuse reflectance spectra of RGO/$ZnIn_2S_4$ nanocomposites were displayed in Figure 7. Pure $ZnIn_2S_4$ shows an absorption edge at about 540 nm and its energy gap is estimated to be 2.4 eV.[7] Although the incorporation of RGO onto $ZnIn_2S_4$ does not obviously change the band gap of $ZnIn_2S_4$, attributable to the absorption of RGO, enhanced absorption in the visible light region is observed in the resultant RGO/$ZnIn_2S_4$ nanocomposites. The absorption intensity of RGO/$ZnIn_2S_4$ nanocomposites in the visible light region increases with the amount of RGO incorporated, in agreement with the observed color change from yellow to dark green of the samples.[35]

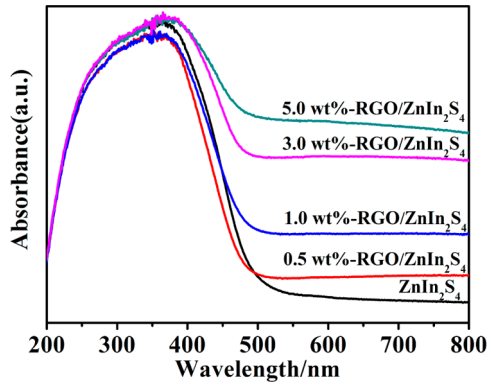

Figure 7. UV−vis DRS spectra of pure $ZnIn_2S_4$ and RGO/$ZnIn_2S_4$ nanocomposites with different amount of RGO.

Photocatalytic hydrogen evolution experiments were carried out over the as-prepared RGO/$ZnIn_2S_4$ nanocomposites in the presence of lactic acid as sacrificial agent under visible light irradiations. It was found that pure $ZnIn_2S_4$ only had a low activity, with the amount of hydrogen evolved determined to be 57.0 μmol in 6 h. However, a significant improvement of the photocatalytic activity was observed when $ZnIn_2S_4$ was incorporated with a little amount of RGO. 160.5 μmol of hydrogen was evolved over 0.5 wt %-RGO/$ZnIn_2S_4$ nanocomposite, about 2.8 times of that over pure $ZnIn_2S_4$ under otherwise similar condition (Figure 8a). The time-dependent hydrogen evolution over 1.0 wt %-RGO/$ZnIn_2S_4$ nanocomposite, pure $ZnIn_2S_4$, and RGO was shown in Figure 8b. It was found that the amount of hydrogen evolved increase with the irradiations time, and the amount of hydrogen evolved reach 245.1 μmol in 6 h over 1.0 wt %-RGO/$ZnIn_2S_4$ nanocomposite, an almost 4.3 times as that obtained over the pure $ZnIn_2S_4$. The effect of the amount of RGO incorporated on the photocatalytic performance of the RGO/$ZnIn_2S_4$ nanocomposites has also been investigated and the results are shown in Figure 8a. The rate of hydrogen evolution first increases with the amount of the incorporated RGO and an optimum hydrogen evolution is observed over 1.0 wt %-RGO/$ZnIn_2S_4$. However a further increase in the amount of RGO results in a decrease of the photocatalytic hydrogen evolution rate. A decrease in the photocatalytic activity over samples with a heavy loading of RGO is likely due to the shading effect of RGO. When covered with RGO, the light absorption by $ZnIn_2S_4$ will be partly blocked and the inefficient excitation of $ZnIn_2S_4$ will lead to the decrease of the photocatalytic performance. Such a shading effect has already been reported previously.[17,25] Therefore, an appropriate RGO loading amount is crucial to achieve the optimized photocatalytic activity of $ZnIn_2S_4$ photocatalyst.

The mechanism for the enhanced photocatalytic hydrogen evolution over the as-prepared sheet-on-sheet RGO/$ZnIn_2S_4$ nanocomposites under visible light irradiation was proposed in Scheme 2. Although the conduction band edge of $ZnIn_2S_4$ (−1.1 eV) is higher than the reduction potential of H^+/H_2, the photocatalytic activity for hydrogen evolution is low over bare $ZnIn_2S_4$ due to the rapid recombination of photogenerated charge carriers as well as the presence of a large hydrogen evolution overpotential. The incorporation of RGO into $ZnIn_2S_4$ can lead to an effective hole−electron separation due to an electron transfer from the CB of $ZnIn_2S_4$ to RGO. The strong interaction between the RGO and $ZnIn_2S_4$ in the as-

dx.doi.org/10.1021/am5004415 | ACS Appl. Mater. Interfaces 2014, 6, 3483−3490

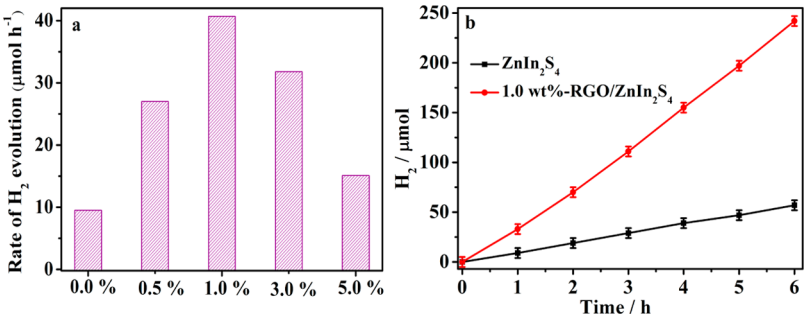

Figure 8. (a) Hydrogen evolution rate over $ZnIn_2S_4$ and RGO/$ZnIn_2S_4$ with different RGO loading amount. (b) Time-dependent hydrogen evolution over 1.0 wt %-RGO/$ZnIn_2S_4$ nanocomposite and pure $ZnIn_2S_4$.

Scheme 2. Schematic Illustration for the Enhanced Photocatalytic Hydrogen Evolution over RGO/$ZnIn_2S_4$ Nanocomposites

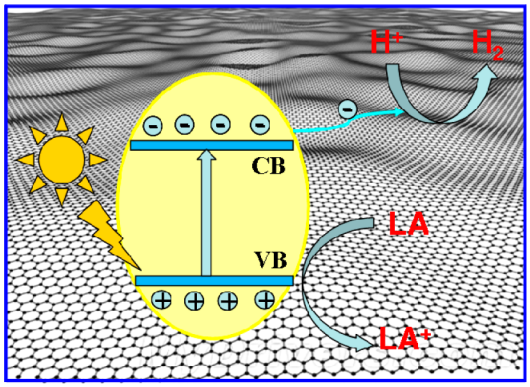

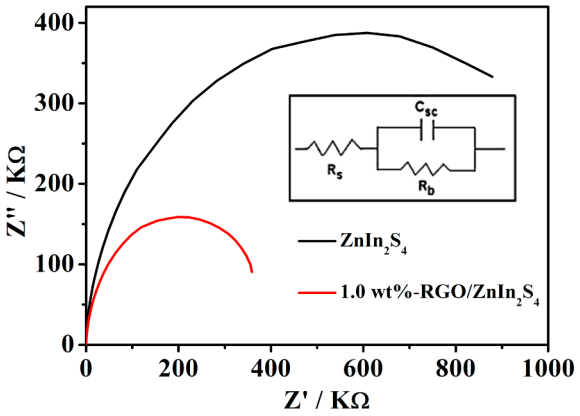

Figure 9. Nyquist plots of experimental impedance data for $ZnIn_2S_4$ and 1.0 wt %-RGO/$ZnIn_2S_4$ nanocomposite in the frequency range of $0.01-1.0\times10^5$ Hz using an ac bias of 0 V vs Ag/AgCl without visible light irradiations in 0.2 M Na_2SO_4 aqueous solution. Inset: Electrical equivalent circuit used for fitting of impedance spectra. R_s, C_{sc}, and R_b represent electrolyte resistance, space charge capacitance, and bulk electrode resistance, respectively.

prepared RGO/$ZnIn_2S_4$ nanocomposite can ensure an effective electron transfer from $ZnIn_2S_4$ to RGO.[22,29,42] In addition, since RGO has previously been shown to be an electrocatalyst for hydrogen evolution, RGO can also act as a non-noble-metal cocatalyst like some transition metal chalcogenides.[18,43−45] The photogenerated electrons transferred to RGO can further move to the defective carbon sites which act as active hydrogen evolution sites to reduce H_2O. Such an electron transportation process, in part determined by their electronic conductivity, can significantly influence the photocatalytic performance of these RGO nanocomposites photocatalysts. Actually, previous study has revealed a correlation between the performance of photocatalytic hydrogen evolution and the RGO reduction degree over RGO/$ZnIn_2S_4$ photocatalytic nanocomposites. As shown in Figure 9, the electrochemical impedance spectra (EIS) analysis reveals that the solvothermal prepared 1.0 wt %-RGO/$ZnIn_2S_4$ nanocomposite shows smaller semicircle as compared with that of pure $ZnIn_2S_4$, suggesting its superior electronic conductivity. In addition, the XPS result suggests that the RGO in the as-prepared RGO/$ZnIn_2S_4$ nanocomposites are highly reductive, which can benefit the charge transfer in the RGO/$ZnIn_2S_4$ system. Since photoluminescence (PL) spectra is generally utilized to investigate the recombination rate of the photo-generated charger carriers,[46−48] the PL spectra of pure $ZnIn_2S_4$ and RGO/$ZnIn_2S_4$ with different amount of RGO have also been investigated (Supporting Information Figure S5). The intensity of the PL peak on RGO/$ZnIn_2S_4$ nanocomposites decreases as compared to that of pure $ZnIn_2S_4$, indicating the incorporation of RGO leads to a decrease of the recombination rate in the nanocomposites. Besides this, the 1.0 wt %-RGO/$ZnIn_2S_4$ nanocomposite shows the lowest PL intensity, in agreement with its highest photocatalytic activity. Therefore, the highly reductive RGO in the RGO/$ZnIn_2S_4$ nanocomposites can serve as a good electron acceptor, mediator as well as the co-catalyst, which contributes to their highly enhanced photocatalytic performance for photocatalytic H_2 generation. However, too much RGO can have a shading effect and can lead to a decrease of hydrogen evolution rate as observed over 5.0 wt %-RGO/$ZnIn_2S_4$ nanocomposite.

4. CONCLUSION

In summary, a facile one-pot solvothermal method has been developed for the preparations of RGO/$ZnIn_2S_4$ nanocomposites with $ZnIn_2S_4$ nanosheets grown on the surface of highly reductive RGO. The highly reductive RGO in the RGO/$ZnIn_2S_4$ nanocomposites serves as a good electron acceptor and mediator, as well as the co-catalyst, which contributes to the highly enhanced photocatalytic performance for photocatalytic hydrogen evolution over the as-prepared RGO/$ZnIn_2S_4$ nanocomposites. This study can provide some guidance for us in the developing of other RGO-incorporated nanocomposite photocatalysts.

dx.doi.org/10.1021/am5004415 | ACS Appl. Mater. Interfaces 2014, 6, 3483−3490

■ ASSOCIATED CONTENT

Supporting Information

Additional characterizations, time-dependent experiments, and PL spectra. This information is available free of charge via the Internet at http://pubs.acs.org/.

■ AUTHOR INFORMATION

Corresponding Author

*E-mail: zhaohuili1969@yahoo.com. Tel (Fax): 86-591-83779260.

Notes

The authors declare no competing financial interest.

■ ACKNOWLEDGMENTS

The work was supported by NSFC (21273035, 21077023), 973 Programs (2014CB239303), and Specialized Research Fund for the Doctoral Program of Higher Education (20123514110002). Z.L. thanks the Award Program for Minjiang Scholar Professorship for financial support.

■ REFERENCES

(1) Chen, X.; Shen, S.; Guo, L.; Mao, S. S. Semiconductor-Based Photocatalytic Hydrogen Generation. *Chem. Rev.* **2010**, *110*, 6503−6570.

(2) Tong, H.; Ouyang, S. X.; Bi, Y. P.; Umezawa, N.; Oshikiri, M.; Ye, J. H. Nano-Photocatalytic Materials: Possibilities and Challenges. *Adv. Mater.* **2012**, *24*, 229−251.

(3) Fujishima, A.; Honda, K. Electrochemical Photolysis of Water at a Semiconductor Electrode. *Nature* **1972**, *238*, 37−38.

(4) Zhang, J.; Xu, Q.; Feng, Z.; Li, M.; Li, C. Importance of the Relationship between Surface Phases and Photocatalytic Activity of TiO_2. *Angew. Chem. Int. Ed.* **2008**, *47*, 1766−1769.

(5) Tsuji, I.; Kato, H.; Kobayashi, H.; Kudo, A. Photocatalytic H_2 Evolution Reaction from Aqueous Solutions over Band Structure-Controlled $(AgIn)_xZn_{2(1-x)}S_2$ Solid Solution Photocatalysts with Visible-Light Response and Their Surface Nanostructures. *J. Am. Chem. Soc.* **2004**, *126*, 13406−13413.

(6) Maeda, K.; Takata, T.; Hara, M.; Saito, N.; Inoue, Y.; Kobayashi, H.; Domen, K. GaN:ZnO Solid Solution as a Photocatalyst for Visible-Light-Driven Overall Water Splitting. *J. Am. Chem. Soc.* **2005**, *127*, 8286−8287.

(7) Lei, Z. B.; You, W. S.; Liu, M. Y.; Zhou, G. H.; Takata, T.; Hara, M.; Domen, K.; Li, C. Photocatalytic Water Reduction under Visible Light on a Novel $ZnIn_2S_4$ Catalyst Synthesized by Hydrothermal Method. *Chem. Commun.* **2003**, *17*, 2142−2143.

(8) Chen, Y. J.; Ge, H.; Wei, L.; Li, Z. H.; Yuan, R. S.; Liu, P.; Fu, X. Z. Reduction Degree of Reduced Graphene Oxide (RGO) Dependence of Photocatalytic Hydrogen Evolution Performance over RGO/$ZnIn_2S_4$ Nanocomposites. *Catal. Sci. Technol.* **2013**, *3*, 1712−1717.

(9) Wang, X.; Maeda, K.; Thomas, A.; Takanabe, K.; Xin, G.; Carlsson, J.; Domen, K.; Antonietti, M. A Metal-Free Polymeric Photocatalyst for Hydrogen Production from Water under Visible Light. *Nat. Mater.* **2009**, *8*, 76−80.

(10) Luo, W.; Yang, Z.; Li, Z.; Zhang, J.; Liu, J.; Zhao, Z.; Wang, Z.; Yan, S.; Yu, T.; Zou, Z. Solar Hydrogen Generation from Seawater with a Modified $BiVO_4$ Photoanode. *Energy Environ. Sci.* **2011**, *4*, 4046−4051.

(11) Zhang, J.; Wang, Y.; Zhang, J.; Lin, Z.; Huang, F.; Yu, J. Enhanced Photocatalytic Hydrogen Production Activities of Au-Loaded ZnS Flowers. *ACS Appl. Mater. Interfaces* **2013**, *5*, 1031−1037.

(12) Zheng, L.; Xu, Y.; Song, Y.; Wu, C.; Zhang, M.; Xie, Y. Nearly Monodisperse $CuInS_2$ Hierarchical Microarchitectures for Photocatalytic H_2 Evolution under Visible Light. *Inorg. Chem.* **2009**, *48*, 4003−4009.

(13) Kudo, A.; Miseki, Y. Heterogeneous Photocatalyst Materials for Water Splitting. *Chem. Soc. Rev.* **2009**, *38*, 253−278.

(14) Chen, Z. X.; Li, D. Z.; Zhang, W. J.; Chen, C.; Li, W. J.; Sun, M.; He, Y. H.; Fu, X. Z. Low-Temperature and Template-Free Synthesis of $ZnIn_2S_4$ Microspheres. *Inorg. Chem.* **2008**, *47*, 9766−9772.

(15) Chen, Y.; Hu, S.; Liu, W.; Chen, X.; Wu, L.; Wang, X.; Liu, P.; Li, Z. Controlled Syntheses of Cubic and Hexagonal $ZnIn_2S_4$ Nanostructures with Different Visible-Light Photocatalytic Performance. *Dalton Trans.* **2011**, *40*, 2607−2613.

(16) Chen, Y.; Huang, R.; Chen, D.; Wang, Y.; Liu, W.; Li, X.; Li, Z. Exploring the Different Photocatalytic Performance for Dye Degradations over Hexagonal $ZnIn_2S_4$ Microspheres and Cubic $ZnIn_2S_4$ Nanoparticles. *ACS Appl. Mater. Interfaces* **2012**, *4*, 2273−2279.

(17) Zhou, J.; Tian, G.; Chen, Y.; Meng, X.; Shi, Y.; Cao, X.; Pana, K.; Fu, H. In Situ Controlled Growth of $ZnIn_2S_4$ Nanosheets on Reduced Graphene Oxide for Enhanced Photocatalytic Hydrogen Production Performance. *Chem. Commun.* **2013**, *49*, 2237−2239.

(18) Wei, L.; Chen, Y.; Lin, Y.; Wu, H.; Yuan, R.; Li, Z. MoS_2 as Non-Noble-Metal Co-catalyst for Photocatalytic Hydrogen Evolution over Hexagonal $ZnIn_2S_4$ under Visible Light Irradiations. *Appl. Catal. B: Environ.* **2014**, *144*, 521−527.

(19) Shen, S.; Zhao, L.; Zhou, Z.; Guo, L. Enhanced Photocatalytic Hydrogen Evolution over Cu-Doped $ZnIn_2S_4$ under Visible Light Irradiation. *J. Phys. Chem. C* **2008**, *112*, 16148−116155.

(20) Chai, B.; Peng, T.; Zeng, P.; Zhang, X. Preparation of a MWCNTs/$ZnIn_2S_4$ Composite and Its Enhanced Photocatalytic Hydrogen Production under Visible-Light Irradiation. *Dalton Trans.* **2012**, *41*, 1179−1186.

(21) Peng, S.; Zhu, P.; Mhaisalkar, S. G.; Ramakrishna, S. Self-Supporting Three-Dimensional $ZnIn_2S_4$/PVDF-Poly (MMA-co-MAA) Composite Mats with Hierarchical Nanostructures for High Photocatalytic Activity. *J. Phys. Chem. C* **2012**, *116*, 13849−13857.

(22) Lightcap, I. V.; Koseland, T. H.; Kamat, P. V. Anchoring Semiconductor and Metal Nanoparticles on a Two-Dimensional Catalyst Mat. Storing and Shuttling Electrons with Reduced Graphene Oxide. *Nano Lett.* **2010**, *10*, 577−583.

(23) Geim, A. K.; Novoselov, K. S. The Rise of Graphene. *Nat. Mater.* **2007**, *6*, 183−191.

(24) Zhang, Y.; Tan, Y.; Stormer, H. L.; Kim, P. Experimental Observation of the Quantum Hall Effect and Berry's Phase in Graphene. *Nature* **2005**, *438*, 201−204.

(25) Jia, L.; Wang, D. H.; Huang, Y. X.; Xu, A. W.; Yu, H. Q. Highly Durable N-Doped Graphene/CdS Nanocomposites with Enhanced Photocatalytic Hydrogen Evolution from Water under Visible Light Irradiation. *J. Phys. Chem. C* **2011**, *115*, 11466−11473.

(26) Wang, J.; Tsuzuki, T.; Tang, B.; Hou, X.; Sun, L.; Wang, X. Reduced Graphene Oxide/ZnO Composite: Reusable Adsorbent for Pollutant Management. *ACS Appl. Mater. Interfaces* **2012**, *4*, 3084−3090.

(27) Xiang, Q.; Yu, J.; Jaroniec, M. Graphene-Based Semiconductor Photocatalysts. *Chem. Soc. Rev.* **2012**, *41*, 782−796.

(28) Hummers, W. S.; Offeman, R. E. Preparation of Graphitic Oxide. *J. Am. Chem. Soc.* **1958**, *80*, 1339.

(29) Li, Q.; Guo, B. D.; Yu, J. G.; Ran, J. R.; Zhang, B. H.; Yan, H. J.; Gong, J. R. Highly Efficient Visible-Light-Driven Photocatalytic Hydrogen Production of CdS-Cluster-Decorated Graphene Nanosheets. *J. Am. Chem. Soc.* **2011**, *133*, 10878−10884.

(30) Li, H. F.; Yu, H.; Chen, S.; Zhao, H.; Zhang, Y.; Quan, X. Fabrication of Graphene Wrapped $ZnIn_2S_4$ Microspheres Heterojunction with Enhanced Interfacial Contact and Its Improved Photocatalytic Performance. *Dalton Trans.* **2013**, DOI: 10.1039/c3dt52820k.

(31) Shen, J. F.; Yan, B.; Shi, M.; Ma, H. W.; Li, N.; Ye, M. X. One Step Hydrothermal Synthesis of TiO_2-Reduced Graphene Oxide Sheets. *J. Mater. Chem.* **2011**, *21*, 3415−3421.

(32) Wang, J.; Hernandez, Y.; Lotya, M.; Coleman, J. N.; Blau, W. J. Broadband Nonlinear Optical Response of Graphene Dispersions. *Adv. Mater.* **2009**, *21*, 2430−2435.

(33) Huang, R.; Ge, H.; Lin, X.; Guo, Y.; Yuan, R.; Fu, X.; Li, Z. Facile One-Pot Preparation of α-$SnWO_4$/Reduced Graphene Oxide

(RGO) Nanocomposite with Improved Visible Light Photocatalytic Activity and Anode Performance for Li-Ion Batteries. *RSC Adv.* **2013**, *3*, 1235−1242.
(34) Murugan, A. V.; Muraliganth, T.; Manthiram, A. Rapid, Facile Microwave-Solvothermal Synthesis of Graphene Nanosheets and Their Polyaniline Nanocomposites for Energy Strorage. *Chem. Mater.* **2009**, *21*, 5004−5006.
(35) Stankovich, S.; Dikin, D. A.; Piner, R. D.; Kohlhaas, K. A.; Kleinhammes, A.; Jia, Y. Y.; Wu, Y.; Nguyen, S. T.; Ruoff, R. S. Synthesis of Graphene-Based Nanosheets via Chemical Reduction of Exfoliated Graphite Oxide. *Carbon* **2007**, *45*, 1558−1565.
(36) Iwase, A.; Ng, Y. H.; Ishiguro, Y.; Kudo, A.; Amal, R. Reduced Graphene Oxide as a Solid-State Electron Mediator in Z-Scheme Photocatalytic Water Splitting under Visible Light. *J. Am. Chem. Soc.* **2011**, *133*, 11054−11057.
(37) Park, Y.; Kang, S. H.; Choi, W. Y. Exfoliated and Reorganized Graphite Oxide on Titania Nanoparticles as an Auxiliary Co-catalyst for Photocatalytic Solar Conversion. *Phys. Chem. Chem. Phys.* **2011**, *13*, 9425−9431.
(38) Peng, S.; Wu, Y. Z.; Zhu, P.; Thavasi, V.; Ramakrishna, S.; Mhaisalkar, S. G. Controlled Synthesis and Photoelectric Application of $ZnIn_2S_4$ Nanosheet/TiO_2 Nanoparticle Composite Films. *J. Mater. Chem.* **2011**, *21*, 15718−15726.
(39) Dubin, S.; Gilje, S.; Wang, K.; Tung, V.; Cha, K.; Hall, A.; Farrar, J.; Varshneya, R.; Yang, Y.; Kaner, R. A One-Step, Solvothermal Reduction Method for Producing Reduced Graphene Oxide Dispersions in Organic Solvents. *ACS Nano* **2010**, *4*, 3845−3852.
(40) Villar-Rodil, S.; Paredes, J. I.; Martinez-Alonso, A. J.; Tascon, M. D. Preparation of Graphene Dispersions and Graphene−Polymer Composites in Organic Media. *J. Mater. Chem.* **2009**, *19*, 3591−3593.
(41) Wang, H.; Robinson, J. T.; Li, X.; Dai, H. Solvothermal Reduction of Chemically Exfoliated Graphene Sheets. *J. Am. Chem. Soc.* **2009**, *131*, 9910−9911.
(42) Zhang, X. Y.; Li, H. P.; Cui, X. L.; Lin, Y. H. Graphene/TiO_2 Nanocomposites: Synthesis, Characterization and Application in Hydrogen Evolution from Water Photocatalytic Splitting. *J. Mater. Chem.* **2010**, *20*, 2801−2806.
(43) Zong, X.; Yan, H. J.; Wu, G. P.; Ma, G. J.; Wen, F. Y.; Wang, L.; Li, C. Enhancement of Photocatalytic H_2 Evolution on CdS by Loading MoS_2 as Cocatalyst under Visible Light Irradiation. *J. Am. Chem. Soc.* **2008**, *130*, 7176−7177.
(44) Xiang, Q. J.; Yu, J. G.; Jaroniec, M. Synergetic Effect of MoS_2 and Graphene as Cocatalysts for Enhanced Photocatalytic H_2 Production Activity of TiO_2 Nanoparticles. *J. Am. Chem. Soc.* **2012**, *134*, 6575−6578.
(45) Zhang, W.; Wang, Y. B.; Wang, Z.; Zhong, Z. Y.; Xu, R. Highly Efficient and Noble Metal-Free NiS/CdS Photocatalysts for H_2 Evolution from Lactic Acid Sacrificial Solution under Visible Light. *Chem. Commun.* **2010**, *46*, 7631−7633.
(46) Cao, J.; Xu, B. B.; Luo, B. D.; Lin, H. L.; Chen, S. F. Novel BiOI/BiOBr Heterojunction Photocatalysts with Enhanced Visible Light Photocatalytic Properties. *Catal. Commun.* **2011**, *13*, 63−68.
(47) Yue, W. J.; Han, S. K.; Peng, R. X.; Shen, W.; Geng, H. W.; Wu, F.; Tao, S. W.; Wang, M. T. $CuInS_2$ Quantum Dots Synthesized by a Solvothermal Route and Their Application as Effective Electron Acceptors for Hybrid Solar Cells. *J. Mater. Chem.* **2010**, *20*, 7570−7578.
(48) Liang, N.; Zai, J.; Xu, M.; Zhu, Q.; Wei, X.; Qian, X. Novel Bi_2S_3/$Bi_2O_2CO_3$ Heterojunction Photocatalysts with Enhanced Visible Light Responsive Activity and Wastewater Treatment. *J. Mater. Chem. A* **2013**, DOI: 10.1039/C3TA13931J.